Photon transition tuning in bulk IV-VI materials

We investigated the dependence of bulk IV-VI material energy levels on the energy gap E_g and composition *x* using a four band k.p model. When paramagnetic ions such as Eu or Mn are introduced, exchange effects are present and the system is described by the simplified Hamiltonian[1]

$$\begin{pmatrix} \frac{-E_g}{2} + (a_1 - a_2)\cos\varphi & a_1 \sin\varphi & 0 & 0 \\ a_1 \sin\varphi & \frac{-E_g}{2} - (a_1 - a_2)\cos\varphi & 0 & 0 \\ 0 & 0 & \frac{E_g}{2} + (b_1 - b_2)\cos\varphi & -b_1 \sin\varphi \\ 0 & 0 & -b_1 \sin\varphi & \frac{E_g}{2} - (b_1 - b_2)\cos\varphi \end{pmatrix} \quad (1)$$

Where we have assumed zero external magnetic field and zero momentum. The angle φ is between the longitudinal direction, chosen to be [111], and the magnetization direction.

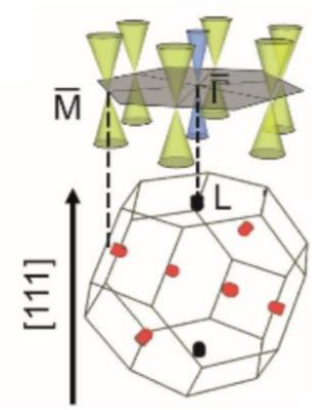

The anisotropy of the system means that the Fermi surfaces at the band extrema form ellipsoids which are elongated perpendicular to the surface of the Brillouin zone. Band extrema are at the L points, so in the Brillouin zone construction shown to the right, the valleys at black points form with their major axis parallel to the [111], while the valleys at red points form an angle $\varphi = 1.23$ radians. The former are referred to as longitudinal valleys and the latter oblique valleys.

The terms $a_1,\ a_2, b_1,\ b_2,$ are called exchange parameters and encapsulate the effects of the paramagnetic ions in the material. Their physical definition is given in Reference 1, and experimental results for their values are also obtained. These are reproduced below for $Pb_{1-x}Mn_xTe$ and $Pb_{1-x}Eu_xSe$.[1]

	T (K)	*A* (meV)	a_1 (meV)	*B* (meV)	b_1 (meV)
Mn content					
$x = 0.010$	1.8	-182 ± 15	-288 ± 15	-33 ± 10	27 ± 5
$x = 0.008$	1.8	-192 ± 15	-315 ± 15	-66 ± 10	55 ± 5
$x = 0.006$	1.8	-225 ± 15	-314 ± 15		50 ± 5
$x = 0.006$	3.5	-142 ± 15	-279 ± 15	-41 ± 10	50 ± 5
$x = 0.006$	4.4	-124 ± 15	-279 ± 15	-51 ± 10	51 ± 5
$x = 0.006$	12.0	-51 ± 15	-288 ± 15		59 ± 5
Eu content					
$x = 0.0142$	1.7	32 ± 3	30 ± 3	6.6 ± 1.6	7.5 ± 1.6
$x = 0.024$	1.7	24.4 ± 3	20 ± 3	6 ± 1.6	2.5 ± 1.6
$x = 0.024$	6.0	24 ± 3	18 ± 3	7.8 ± 1.6	0.9 ± 1.6
$x = 0.024$	12.0	22 ± 3	17.5 ± 3	9.7 ± 1.6	2.2 ± 1.6

The parameters $A = a_1 - a_2$ and $B = b_1 - b_2$ have been measured but the conversion is simple. Using these results, it is straightforward to determine the dependence of the energy levels on the band gap. Plots of this dependence for the various $Pb_{1-x}Eu_xSe$ data sets are shown in Figures 1-4 below.

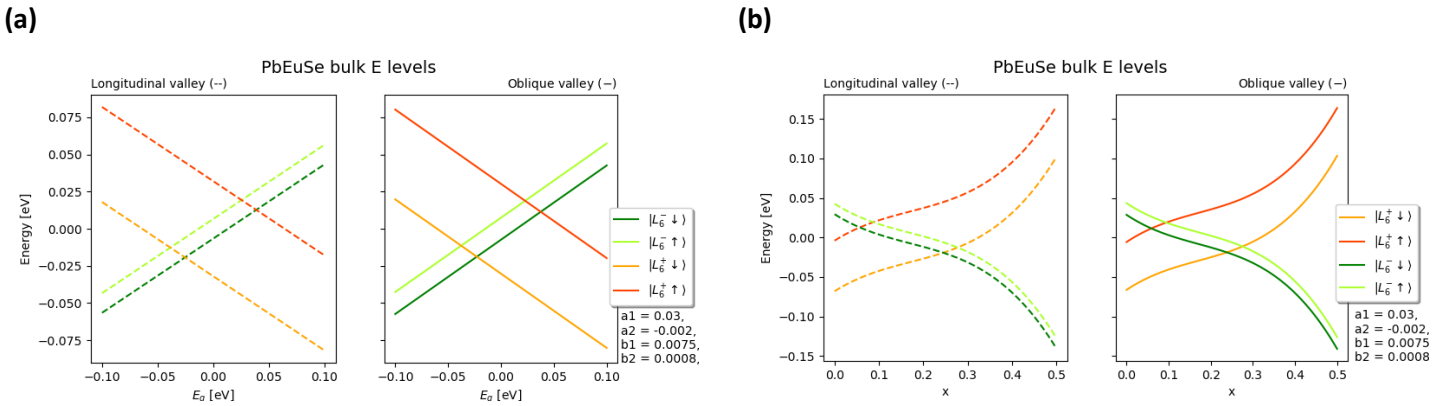

FIG. 1: x = 0.0142, T = 1.7 K. Energy levels vs **(a)** energy gap and **(b)** Eu composition. Intervalley energy differences $\delta E = E_{\varphi=0} - E_{\varphi=1.23}$ are $\delta E(L_6^- \uparrow) = 0.8\ \text{meV},\ \delta E(L_6^- \downarrow) = -0.8\ \text{meV},\ \delta E(L_6^+ \uparrow) = 1.8\ \text{meV},\ \delta E(L_6^+ \downarrow) = -1.8\ \text{meV}.$

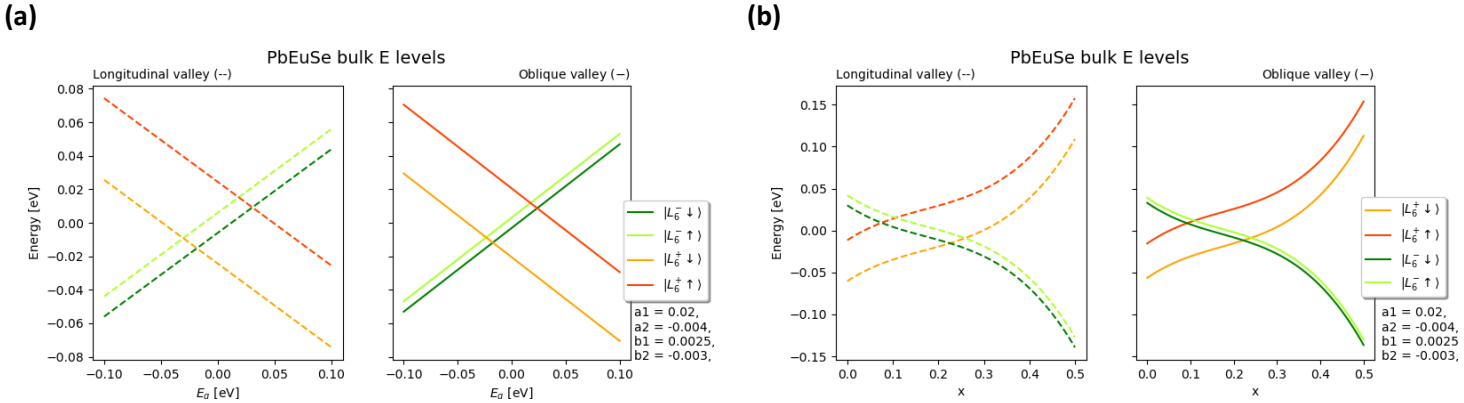

FIG. 2: x = 0.024, T = 1.7 K. Energy levels vs **(a)** energy gap and **(b)** Eu composition. Intervalley energy differences are $\delta E(L_6^- \uparrow) = -8.1\ \text{meV},\ \delta E(L_6^- \downarrow) = 8.1\ \text{meV},\ \delta E(L_6^+ \uparrow) = 17.7\ \text{meV},\ \delta E(L_6^+ \downarrow) = -17.7\ \text{meV}.$

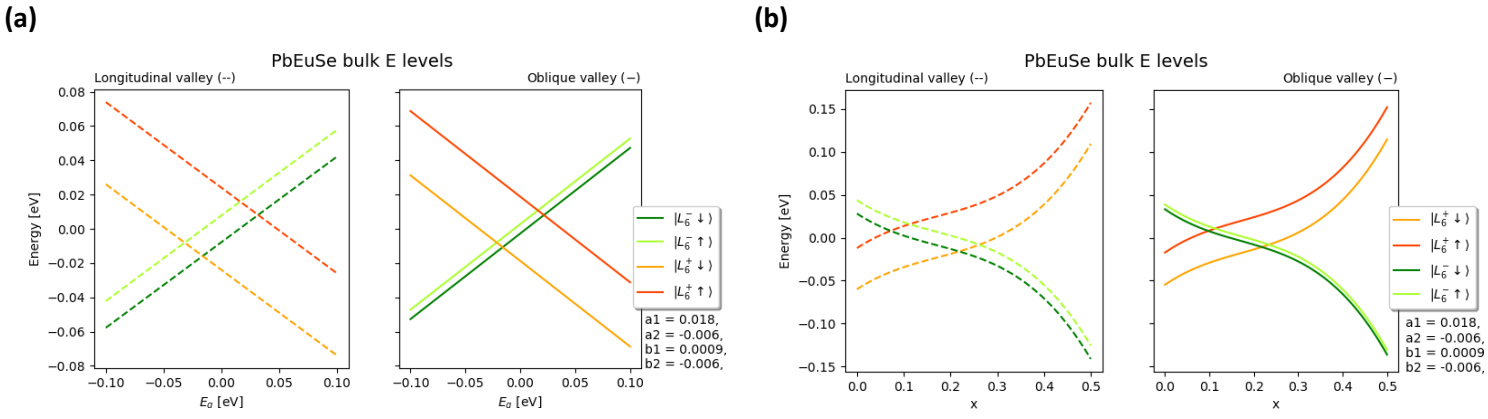

FIG. 3: x = 0.024, T = 6.0 K. Energy levels vs **(a)** energy gap and **(b)** Eu composition. Intervalley energy differences are $\delta E(L_6^- \uparrow) = -40.3\ \text{meV},\ \delta E(L_6^- \downarrow) = 40.3\ \text{meV},\ \delta E(L_6^+ \uparrow) = 88.5\ \text{meV},\ \delta E(L_6^+ \downarrow) = -88.5\ \text{meV}.$

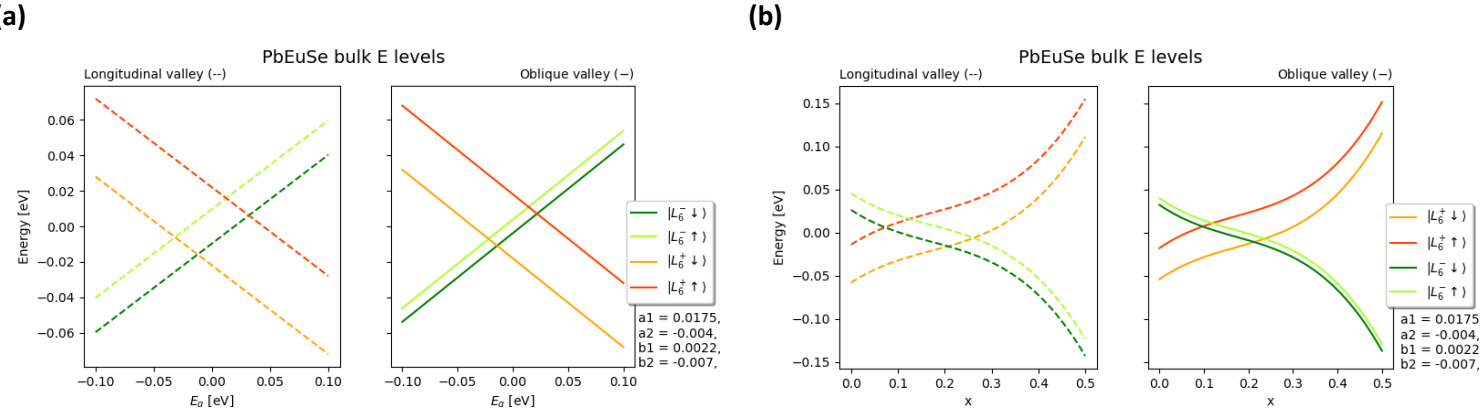

FIG. 4: x = 0.024, T = 12.0 K. Energy levels vs **(a)** energy gap and **(b)** Eu composition. Intervalley energy differences are $\delta E(L_6^- \uparrow) = -80.5\ \text{meV},\ \delta E(L_6^- \downarrow) = 80.5\ \text{meV},\ \delta E(L_6^+ \uparrow) = 177.1\ \text{meV},\ \delta E(L_6^+ \downarrow) = -177.1\ \text{meV}.$

In general both valleys have the same linear E_g dependence because they share the same $\frac{\pm E_g}{2}$ terms along the diagonal of the bulk Hamiltonian. However, each are shifted due to the exchange effects, the central valley levels with a simple $\pm A$ or $\pm B$ shift due to the fact that $\sin\varphi = 0$ for this valley and the oblique valley levels with a more complicated shift that includes off diagonal components.

Physically, we are interested in the γ absorption spectrum of the material. Only transitions with $\Delta s = 0$ are allowed. Therefore in the two-band model only the $|L_6^+ \uparrow\rangle \rightarrow |L_6^- \uparrow\rangle$ and $|L_6^+ \downarrow\rangle \rightarrow |L_6^- \downarrow\rangle$ transitions are allowed and the absorbed photon energy $E_g = \Delta E$ will be band gap dependent in each case. We can use the results calculated above to arrive at these transition energies. We are particularly interested in the case that a particular transition in one valley has the same energy as its spin opposite transition in the other valley, i.e. $E(|L_6^+ \uparrow, \varphi = 0\rangle \rightarrow |L_6^- \uparrow, \varphi = 0\rangle) = E(|L_6^+ \downarrow, \varphi = 1.23\rangle \rightarrow |L_6^- \downarrow, \varphi = 1.23\rangle)$. Such a condition can be satisfied by plotting the photon energies ΔE for each allowed transition of each valley against energy gap and looking for the appropriate intersection points. This is done below for the first $Pb_{1-x}Eu_xSe$ data set. From the Hamiltonian (Equation 1) one can see that in the limit of zero exchange effects, the degeneracy between each valley would not be broken, and the only point of intersection of the transition lines would be at $E_g = 0$. The exchange parameters break the symmetry, and larger and larger parameters push the transition lines for different valleys further and further from each other. This is interesting because it amounts to increasing the magnitude of the gap at which the intersections occur. With this in mind, we looked at the effects of scaling up the exchange parameters by a multiplicative constant. As can be seen in Figure 5, the intersection points are always symmetric about the y axis, in other words occurring at $\pm I$ for contant, positive gap intersection value I. Increasing the scaling factor increases the magnitude of I.

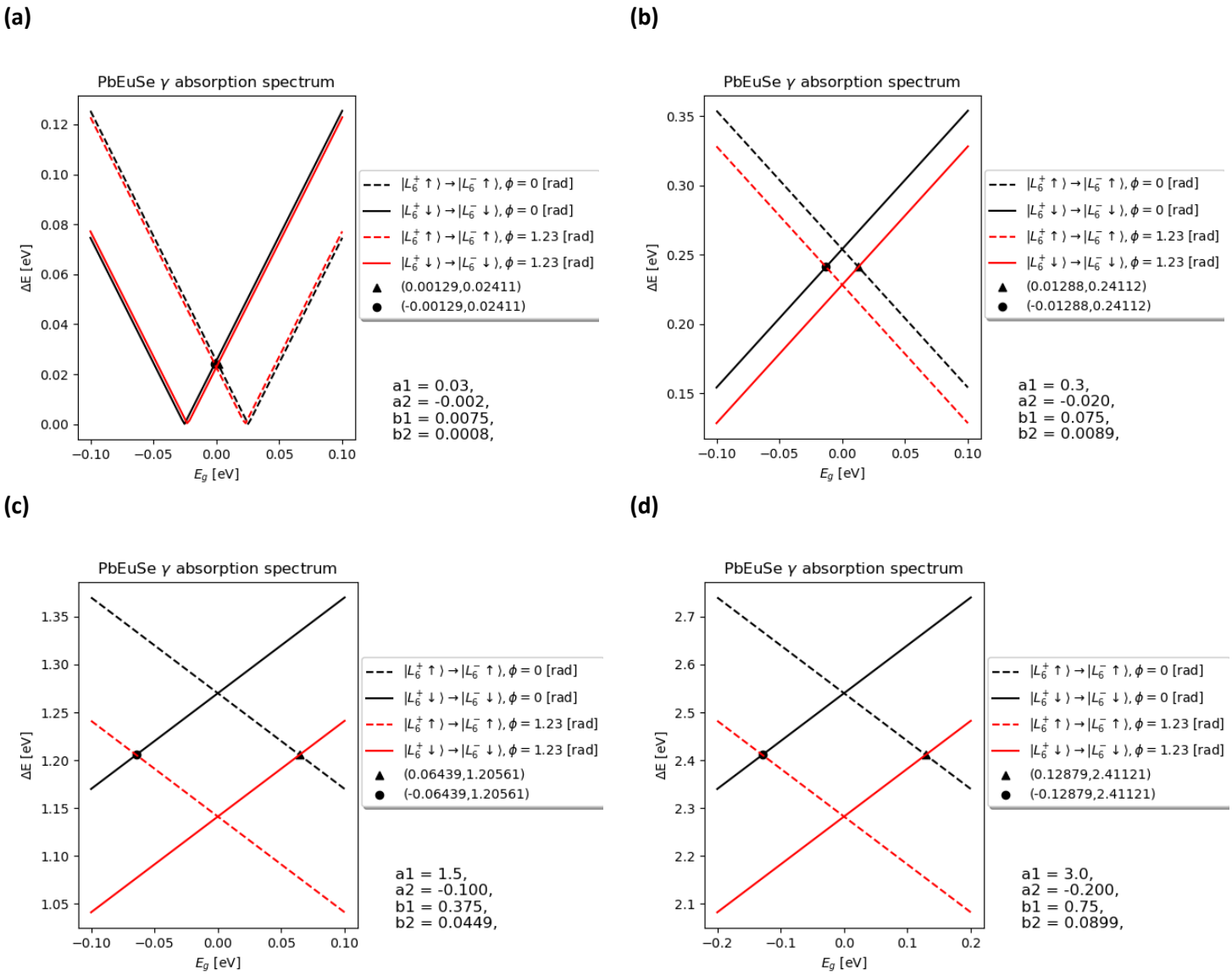

FIG. 5: Photon energies for spin-conserving transitions in both valleys from x = 0.0142, T = 1.7 K data. Intersections of opposite spin, opposite valley lines are determined and marked. **(a)** No scaling factor applied. **(b)** Exchange constants scaled by 10. **(c)** Exchange constants scaled by 50. **(d)** Exchange constants scaled by 100.

We can explore the same effects in the other material explored by Bauer, $Pb_{1-x}Mn_xTe$. The exchange parameters used are larger and hence the intersection points tend to be at larger E_g and ΔE.

(a) **(b)**

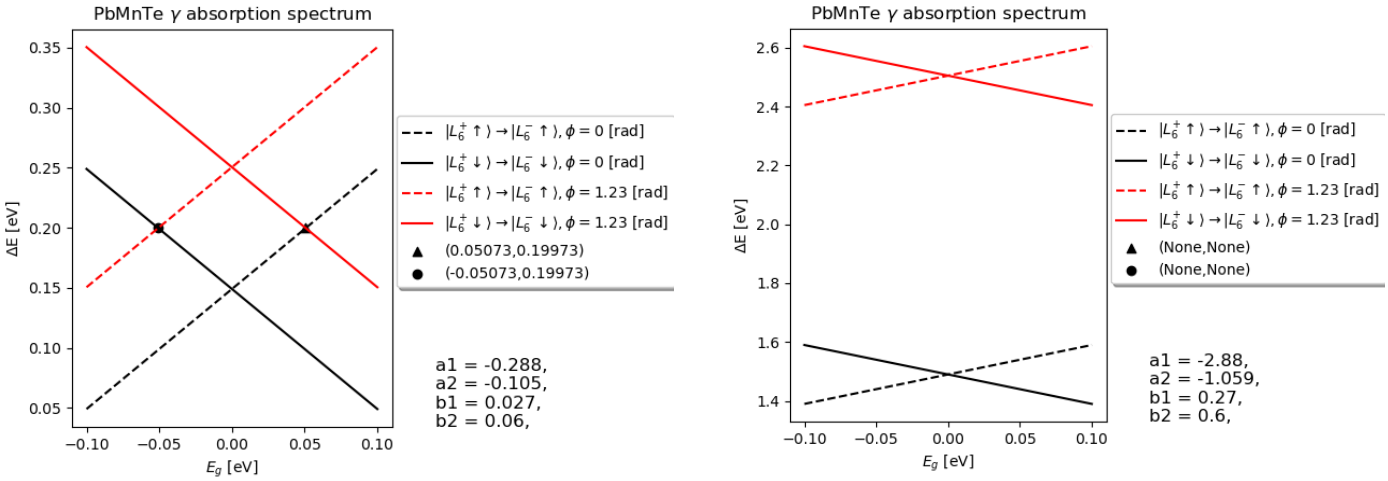

FIG. 6: Photon energies for spin conserving transitions in $Pb_{1-x}Mn_xTe$ from x = 0.01, T = 1.8 K data. Intersections between opposite spin, opposite valley transitions are highlighted as before. **(b)** After a scaling factor of 10 was applied, valley transitions became markedly different from each other such that no intersection was achieved in the domain of interest. As a result, higher scaling factors were not explored.

References

1. Bauer, G et al 1992 *Semicond. Sci. and Technol.* **7** 703.